

Cathodoluminescence of Diamond

Subjects: **Physics, Applied**

Contributor: Evgeny Vasilev

Cathodoluminescence (CL) microscopy revealed heterogeneities in diamonds in a very detailed manner with high spatial resolution.

diamond

cathodoluminescence

FTIR

nitrogen

hydrogen

1. Introduction

Diamond is a crucial mineral for studying the subcontinental lithospheric mantle and sublithospheric horizons [1][2][3]. Diamond crystals record information about their growth conditions and later processes such as deformation by retaining chemical (from uncompromised inclusions) and time–temperature (nitrogen aggregation state) [4][5][6][7][8]. Internal features reveal the complexity of the growth processes of diamonds. The features are visualized via photoluminescence (PL), Fourier transform infrared absorption (FTIR), anomalous birefringence, and cathodoluminescence (CL). CL microscopy provides the most sensitive method for visualizing inhomogeneities in crystals with high resolution and contrast [9][10]. In diamonds, CL reveals zonal and sectorial growth heterogeneities [11][12][13], plastic deformation, and mechanical twinning layers [14][15] as well as irradiation-induced features [16]. More than 300 defects of crystal structure are known in diamond [17]; these appear and transform at all stages of crystal growth [18][19]. These defects are either CL active or they can interact with CL active defects, as such, they can decrease or increase the intensity of the corresponding luminescence systems. The CL spectra of most natural crystals contain a broad structureless band (*A-band*) with a maximum position spaced from 415 to 445 nm [20]. The nature of this system is unclear; evidently, it is related to dislocations and partial sp^2 hybridization [21]. Through defect levels with sp^2 hybridization, electron-hole pair recombination occurs, which manifests itself as the CL *A-band*. This process competes with the recombination of free (*N9* system) and bound (*N10* system) excitons [22]. In crystals with a more perfect structure, the intensity of the *N9* and *N10* systems is high and the intensity of the *A-band* is low [23]. The CL recombination *A-band* is superimposed on the intracenter luminescence of the neutral vacancy, $V(GR1)$, nitrogen vacancy, NV (575 nm), N_2V (*H3*), N_3V (*N3*), N_4V_2 (*H4*) centers, and the broad structureless band of *B'* centers (platelets) [24]. The mechanisms of energy transfer to the PL centers during electron excitation in diamond have been poorly investigated [25][26]. The apparent zoning of crystals is mostly caused by nonuniform distribution of the *A-band* intensity as well as the *N3* and *H3* systems [27]. The concentration of *N3* and *H3* defects is limited by the nitrogen content in the form of N_2 (*A*) [28] and N_4V (*B*) [29] defects. The *N3* defect arises during $A \rightarrow B$ transformation, and *H3* occurs as a result of plastic deformation and irradiation. N_3VH is the common defect in diamond [30]. Notably, four impurity atoms replace four carbon atoms in the model; therefore, the model corresponds to the formula N_3H . The defect is not active in luminescence, but it appears in the FTIR absorption spectra at 3107 cm^{-1} . The nature of its interaction with other defects has not yet been

documented. The intracenter luminescence intensity of the *N*3 and *H*3 systems depends on the concentration of luminescence centers, quenching centers, and perfection of the structure.

2. CL Features in SS-CL and SEM-CL Modes

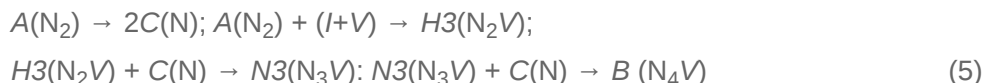
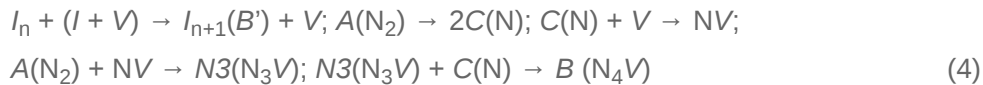
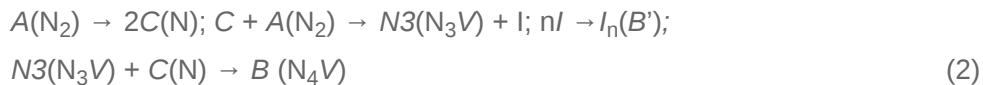
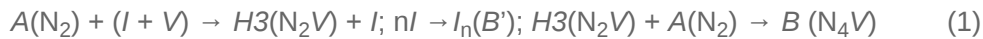
According to the Kanaya–Okayama relation [31], the electron penetration depths in diamond at energies of 20 and 10 KeV were 2.5 and 1 μm , respectively. The CL excitation volume was comparable to the electron penetration depth; therefore, at 10 KeV, the size of the detectable SEM-CL inhomogeneities was approximately 2 μm , which is above the diffraction limit of optical microscopy. The CL locality in scanning mode was determined by the area of CL generation and the diffusion length of the charge carriers. The diffusion length of carriers in the most perfect nitrogen-free crystals is one μm and significantly lower in nitrogen-containing crystals [32].

The advantages of SS-CL optical microscopy are the observation of natural CL colors, weak surface charging effects, and potentially high resolution. Contrast is higher in the SEM-CL mode because of high electron flux density. However, the optimal detection of inhomogeneities depends on the kinetic characteristics of the luminescence because scanning highlights systems with short excitation and attenuation times, whereas steady-state mode highlights systems with long afterglow. Previously, in the study of low-nitrogen crystals, it was established that during pulsed excitation by an electron beam, the *N*3 system has an attenuation time of 30–50 ns, and the *A*-band had an attenuation time of 8–9 ms [27]. Therefore, in the scanning mode, a fast detector registers *N*3 luminescence. The video camera of an optical microscope operates in the SS-CL mode and has long exposure time. Therefore, the intensity of systems with long attenuation time increased. Notably, the probability of radiation-free transitions increased with increasing nitrogen concentration; thus, the attenuation time of the *N*3 system decreased. Therefore, in addition to the spectral sensitivity of the detectors, the kinetic parameters of excitation and the luminescence detection method affect the character of the CL intensity distribution. Fast-decay systems appear stronger in the scanning mode, and the contribution of systems with long decay time increased in the steady-state mode.

In the steady-state mode, reflected light illuminates cracks, inclusions, and surface inhomogeneities and reduces the image contrast. Thus, the brightness of different zones is determined, on one hand, by the admixture composition of diamond, and on the other hand, by the conditions of image acquisition: spectral sensitivity of the photodetector and scanning speed.

3. FTIR Heterogeneity Analysis

It is proposed that the transformation of *A* defects proceeds through intermediate nitrogen-vacancy centers. Calculations showed that the mobility of nitrogen-vacancy centers is significantly higher than that of nitrogen in *C* and *A* defects [33][34]. There are various models (1–5) for the formation of *B* centers, in which nitrogen-vacancy defects are considered as intermediate defects [33][34].



The formation of *B* defects results in the formation of interstitial carbon atoms *I*, which then form *B'* defects—platelets (I_n). In a diamond matrix with dislocations and inclusions, most of the interstitial atoms that form at this stage do not transform into platelets; the carbon atoms flow into dislocations and microinclusions. Therefore, the beginning of the formation of platelets in the $\langle 100 \rangle$ sectors was delayed compared to the $\langle 111 \rangle$ sectors. Due to the low concentration of interstitial atoms, the concentration of platelets in the $\langle 100 \rangle$ sectors was lower than that in the $\langle 111 \rangle$ sectors, but had a larger size. This peculiarity corresponds to the formation of platelets through solid solution decomposition. There seems to be no direct causal relationship in the inverse relationship between a_{3107} and $a_{B'}$. The inverse dependence results from various general regularities: (1) lower hydrogen concentration in the $\langle 111 \rangle$ sectors than in the $\langle 100 \rangle$ sectors; (2) high N_{tot} concentration in the $\langle 111 \rangle$ sectors; and (3) high dislocation and microinclusions density in the sectors $\langle 100 \rangle$. The dependence of a_{B_2} on the nitrogen concentration in form *B* (N_B) is linear [33], whereas the dependence of N_B on N_{tot} is quadratic, which follows from the kinetic equation [29]. Therefore, a difference of 10–20% N_{tot} was accompanied by a difference of 30–40% in $a_{B'}$.

According to the existing models, platelets arise as a drain of interstitial atoms. What reasons alter the kinetics of transformed interstitial carbon atoms in $\langle 100 \rangle$ sectors? Howell et al. [35] suggested that interstitial carbon atoms flow to disc-crack-like defects, a phenomenon found in cuboid diamonds. Not only microinclusions, but also dislocations can be a possible drain for very mobile interstitial carbon atoms, which are characteristic for $\langle 100 \rangle$ sectors [35][36]. The high density of dislocations and microinclusions in the sectors $\langle 100 \rangle$ is caused by the normal mechanism of their growth. The presence of an alternative drain for interstitial atoms significantly affects the formation of platelets. The formation of platelets is described by the kinetics of the decay of the solid solution of interstitial carbon atoms in the diamond matrix [37]. The number of interstitial carbon atoms formed is proportional to the $A \rightarrow B$ reaction rate. Additionally, when the interstitial carbon atoms have an outlet, the concentration of the formed platelets decreases sharply compared to the matrix in which there is no alternate outlet for the interstitial carbon atoms. Two types of diamond matrix with identical thermal history are $\langle 111 \rangle$ and $\langle 100 \rangle$ sectors in mixed-habit crystals. The hydrogen disproportion between the $\langle 111 \rangle$ and $\langle 100 \rangle$ sectors is because of their different growth mechanism. Diamond in the $\langle 111 \rangle$ sectors grows via a layer-by-layer tangential mechanism and via a normal mechanism in the $\langle 100 \rangle$ sectors. The normal or tangential growth mechanism determines the features of

morphology, impurity, and defect composition of crystals. The $<100>$ sectors capture more hydrogen and submicron inclusions, which determines the type and characteristics of the PL and FTIR spectra.

4. Analysis of CL Heterogeneities

In mixed-habit crystals, the CL of the $<100>$ sectors can either be brighter or weaker than that of the $<111>$ sectors under identical observational conditions [38]. In most studies, the CL of the $<100>$ sectors is brighter than that of the $<111>$ sectors [39]. In $<111>$ sectors of crystal 615-66, the *A-band* intensity was twice as high as that in the $<100>$ sectors. In the $<100>$ sectors, the intensity of the *N3* system was high. The intensity of the *N3* system locally decreased around the inclusions, but the intensity of the *A-band* did not change. The decrease in intensity can be attributed to the decrease in the concentration of luminescence centers, quenching by other defects, and general decrease in the perfection of the crystal structure. The concentration of defects can be detected via absorption spectroscopy. However, the detection of absorption spectra in 30 μm areas requires appropriate sample thickness. The phenomenon of decreasing *N3* concentration in the areas of diamond crystal with reduced *N3* system intensity in the SS-SEM CL mode has been previously described [40]. A high concentration of N_3VH was observed in the region without *N3* defects (according to the absorption data). The inverse relationship between the concentrations of *N3* and N_3VH could be attributed to the transformation of the former into the latter during hydrogen atom capture. By considering the phases in the inclusions as a local source of hydrogen, we can write down the equation of $\text{N3} + \text{H} \rightarrow \text{N}_3\text{VH}$ transformation. This equation explains the decrease in the *N3* system intensity in the inclusion region. As shown above, the defect concentration in N_3VH was not related to the degree of nitrogen aggregation from $\text{A} \rightarrow \text{B}$. In neighboring $<100>$ and $<111>$ sectors, the concentration of N_3VH can differ by a factor of 50, but there were no differences in the degree of aggregation of nitrogen between the sectors. Thus, hydrogen atoms transform *N3* centers into N_3VH . Consequently, *N3* defects are not the main intermediate center in the $\text{A} \rightarrow \text{B}$ transformation and form only as one of the side variants of the defect transformation. In the $<100>$ sectors, hydrogen transforms *N3* defects into the N_3VH form, which explains the low intensity of *N3* luminescence.

5. Evolution of Defect Set during Natural Annealing

Comparison of crystals shows that the differences between defect distribution in the $<111>$ and $<100>$ sectors changed during natural annealing and were the highest at the first stage of defect transformation $\text{A} \rightarrow \text{B}$ in crystal 615-66. According to modern concepts, nitrogen atoms are incorporated in the diamond matrix in the form of *C* defects. Thereafter, the *C* defects are transformed into *A* defects. The temperature and time of natural annealing of most crystals are such that all *C* defects transform into form *A*. The next stage of transformation $\text{A} \rightarrow \text{B}$ is achieved in diamond crystals to different degrees. During this stage, concentration of N_3VH increases [41]. In crystals of mixed-habit, the effects influencing transformation of defects have been revealed. The first effect is the influence of the rate of platelet formation; the second effect is the transformation of $\text{N3} \rightarrow \text{N}_3\text{VH}$. During the first stage of natural annealing, there are no platelets in $<100>$ sectors, but they are present in $<111>$ sectors. This difference is greatest in crystals with low aggregation of $\text{A} \rightarrow \text{B}$ defects, and decreases during natural annealing. Because the formation of platelets occurs via solid solution decomposition,

their concentration is low during the first stage of annealing. During further transformation of $A \rightarrow B$ defects, the concentration of platelets does not change, but they increase in size. Therefore, in the $<100>$ pyramids, the concentration of platelets is low but their size is large, and this pattern does not change during further annealing. Therefore, the $<100>$ and $<111>$ sectors differ in the green luminescence intensity of the B' defects. The second effect is explained by the fact that the hydrogen atoms withdraw a part of the intermediate defects, N_3 , from the transformation chain $A \rightarrow B$ and transform them into N_3VH . During prolonged annealing, all hydrogen atoms transform into N_3VH , and the concentration of N_3 defects in the $<100>$ and $<111>$ sectors is equalized. Thus, the differences between the $<100>$ and $<111>$ sectors are greatest during crystal growth, but diminished during prolonged post-growth natural annealing.

References

1. Gurney, J.J.; Helmstaedt, H.H.; Le Roex, A.P.; Nowicki, T.E.; Richardson, S.H.; Westerlund, K.J. Diamonds: Crustal distribution and formation processes in time and space and an integrated deposit model. *Econ. Geol.* 2005, 100, 143–177.
2. Smit, K.V.; Shirey, S.B.; Stern, R.A.; Steele, A.; Wang, W. Diamond growth from C-H-N-O fluids in the lithosphere: Evidence from CH₄ micro-inclusions and ¹³C-¹⁵N-N content in Zimbabwe mixed-habit diamonds. *Lithos* 2016, 265, 68–81.
3. Shirey, S.B.; Smit, K.V.; Pearson, G.D.; Walter, M.J.; Aulbach, S.; Brenker, F.E.; Bureau, H.; Burnham, A.D.; Cartigny, P.; Chacko, T.; et al. Diamonds and the Mantle Geodynamics of Carbon. In Deep Carbon: Past to Present; Orcutt, B., Daniel, I., Dasgupta, R., Eds.; Cambridge University Press: Cambridge, UK, 2019; pp. 89–128. ISBN 9781108677950.
4. Spetsius, Z.V.; Bogush, I.N.; Kovalchuk, O.E. FTIR mapping of diamond plates of eclogitic and peridtotitic xenoliths from the Nyurinskaya pipe, Yakutia: Genetic implications. *Russ. Geol. Geophys.* 2015, 56, 344–353.
5. Stepanov, A.S.; Shatsky, V.S.; Zedgenizov, D.A.; Sobolev, N.V. Causes of variations in morphology and impurities of diamonds from the Udachnaya Pipe eclogite. *Russ. Geol. Geophys.* 2007, 48, 758–769.
6. Bruce, L.F.; Kopylova, M.G.; Longo, M.; Ryder, J.; Dobrzhinetskaya, L.F. Luminescence of diamonds from metamorphic rocks. *Am. Mineral.* 2011, 1, 14–22.
7. Howell, D. Strain-induced birefringence in natural diamond: A review. *Eur. J. Mineral.* 2012, 4, 575–585.
8. Wiggers de Vries, D.F.; Bulanova, G.P.; De Corte, K.; Pearson, D.G.; Craven, J.A.; Davies, G.R. Micron-scale coupled carbon isotope and nitrogen abundance variations in diamonds: Evidence

for episodic diamond formation beneath the Siberian Craton. *Geochim. Cosmochim. Acta* 2013, 100, 176–199.

9. Pagel, M.; Barbin, V.; Blanc, P.; Ohnenstetter, D. Cathodoluminescence in Geosciences: An Introduction. In *Cathodoluminescence in Geosciences*; Pagel, M., Barbin, V., Blanc, P., Ohnenstetter, D., Eds.; Springer: Berlin/Heidelberg, Germany, 2000; ISBN 978-3-662-04086-7.

10. Frelinger, S.N.; Ledvina, M.D.; Kyle, J.R.; Zhao, D. Scanning electron microscopy cathodoluminescence of quartz: Principles, techniques and applications in ore geology. *Ore Geol. Rev.* 2015, 65, 840–852.

11. Hanley, P.L.; Kiflawi, I.; Lang, A.R. On topographically identifiable sources of cathodoluminescence in natural diamonds. *Philos. Trans. R. Soc.* 1977, A284, 329–368.

12. Bulanova, G.P.; Pearson, D.G.; Hauri, E.H.; Griffin, B. Carbon and nitrogen isotope systematics within a sector-growth diamond from the Mir kimberlite, Yakutia. *Chem. Geol.* 2002, 188, 105–123.

13. Titkov, S.; Saparin, G.; Obyden, S. Evolution of growth sectors in natural diamond crystals as revealed by cathodoluminescence topography. *Geol. Ore Depos.* 2002, 44, 350–360.

14. Gaillou, E.; Post, J.E.; Rose, T.R.; Butler, J.E. Cathodoluminescence of Natural, Plastically Deformed Pink Diamonds. *Microsc. Microanal.* 2012, 18, 1292–1302.

15. Gaillou, E.; Post, J.E.; Bassim, N.; Zaitsev, A.M.; Rose, T.R.; Fries, M.D.; Stroud, R.M.; Steele, A.; Butler, J.E. Spectroscopic and microscopic characterization of color lamellae in natural pink diamonds. *Diam. Relat. Mater.* 2010, 19, 1207–1220.

16. Nasdala, L.; Grambole, D.; Wildner, M.; Gigler, A.; Hainschwang, T.; Zaitsev, A.; Harris, J.W.; Milledge, J.; Schulze, D.J.; Hofmeister, W.; et al. Radio-colouration of diamond: A spectroscopic study. *Contrib. Mineral. Petrol.* 2013, 5, 843–861.

17. Dishler, B. *Handbook of Spectral Lines in Diamond*; Springer: Berlin/Heidelberg, Germany, 2001; p. 467.

18. Boyd, S.R.; Matthey, D.P.; Pillinger, C.T.; Milledge, H.J.; Mendelsohn, M.; Seal, M. Multiple growth events during diamond genesis: An integrated study of carbon and nitrogen isotopes and nitrogen aggregation state in coated stones. *Earth Planet Sci. Lett.* 1987, 86, 341–357.

19. Dobrinets, I.A.; Vins, V.G.; Zaitsev, A.M. *HPHT—Treated Diamonds: Diamonds Forever*; Springer: Berlin/Heidelberg, Germany, 2013; p. 276.

20. Ruan, J.; Kobashi, K.; Choyke, W.J. On the “band A” emission and boron related luminescence in diamond. *App. Phys. Lett.* 1992, 25, 3138–3140.

21. Takeuchi, D.; Watanabe, H.; Yamanaka, S.; Okushi, H.; Sawada, H.; Ichinose, H.; Sekiguchi, T.; Kajimura, K. Origin of band-A emission in diamond thin films. *Phys. Rev. B* 2001, 63, 245–328.

22. Robins, L.H.; Farabaugh, E.N.; Feldman, A. Cathodoluminesce spectroscopy of free and bound excitons in chemical-vapor-deposited diamond. *Phys. Rev. B* 1993, 19, 14167–14181.

23. Kawarada, H.; Tsutsumi, T.; Hirayama, H.; Yamaguchi, A. Dominant free—Exciton recombination radiation in chemical vapor deposited diamonds. *Appl. Phys. Lett.* 1994, 4, 451–453.

24. Zaitsev, A.M. Optical Properties of Diamond: Data Handbook; Springer: Berlin/Heidelberg, Germany, 2001; p. 502.

25. Lipatov, E.I.; Genin, D.E.; Grigor'ev, D.; Tarasenko, V.F. Recombination Radiation in the Diamond. In Luminescence—An Outlook on the Phenomena and their Applications; Thirumalai, J., Ed.; Intech Publisher: London, UK, 2016; pp. 191–224. ISBN 978-953-51-2763-5.

26. Panzer, G.; Gaft, M.; Marfunin, A.S. Systems of interacting luminescence centers in natural diamonds: Laser-induced time-resolved and cathodoluminesce spectroscopy. In Cathodoluminescence in Geosciences; Pagel, M., Barbin, V., Blanc, P., Ohnenstetter, D., Eds.; Springer: Berlin/Heidelberg, Germany, 2000; pp. 359–371. ISBN 978-3-662-04086-7.

27. Lipatov, E.I.; Lisitsyn, V.M.; Oleshko, V.I.; Tarasenko, V.F. Spectral and kinetic characteristics of the pulsed cathodoluminescence of a natural IIA-type diamond. *Russ. Phys. J.* 2007, 1, 52–57.

28. Boyd, S.R.; Kiflawi, I.; Woods, G.S. The relationship between infrared absorption and the A defect concentration in diamond. *Philos. Mag. B* 1994, 69, 1149–1153.

29. Boyd, S.R.; Kiflawi, I.; Woods, G.S. Infrared absorption by the B nitrogen aggregate in diamond. *Philos. Mag. B* 1995, 72, 351–361.

30. Goss, J.P.; Briddon, P.R.; Hill, V.; Jones, R.; Rayson, M.J. Identification of the structure of the 3107 cm⁻¹ H-related defect in diamond. *J. Phys. Condens. Matter.* 2014, 26, 1–6.

31. Kanaya, K.; Okayama, S. Penetration and energy loss theory of electrons in solid targets. *J. Phys. D Appl. Phys.* 1972, 5, 43–58.

32. Malinauskas, T.; Jarasiunas, K.; Ivakin, E.; Ralchenko, V.; Gontar, A.; Ivakhnenko, S. Optical evaluation of carrier lifetime and diffusion length in synthetic diamonds. *Diam. Relat. Mater.* 2008, 7–10, 1212–1215.

33. Goss, J.P.; Coomer, B.J.; Jones, R.; Fall, C.; Briddon, P.; Öberg, S. Extended defects in diamond: The interstitial platelet. *Phys. Rev. B* 2003, 67, 165208.

34. Vins, V.G.; Eliseev, A.P. Effect of annealing at high pressures and temperatures on the defect-admixture structure of natural diamonds. *Inorg. Mater. Appl. Res.* 2010, 4, 303–310.

35. Howell, D.; O'Neill, C.J.; Grant, K.J.; Griffin, W.L.; O'Reilly, S.Y.; Pearson, N.J.; Stern, R.A.; Stachel, T. Platelet development in cuboid diamonds: Insights from micro-FTIR mapping. *Contrib. Mineral. Petrol.* 2012, 164, 1011–1025.

36. Zedgenizov, D.; Harte, B.; Shatsky, V.S.; Politov, A.A.; Rylov, G.M.; Sobolev, N.V. Directional chemical variations in diamonds showing octahedral following cuboid growth. *Contrib. Mineral. Petrol.* 2006, 151, 45–57.
37. Vasilyev, E.A.; Sofroneev, S.V. Zoning in diamonds from Mir kimberlite pipe: FTIR data. *Geol. Ore Deposit.* 2008, 8, 784–791.
38. Rondeau, B.; Fritsch, E.; Guiraud, M.; Chalain, J.P.; Notari, F.E. Three historical “asteriated” hydrogen-rich diamonds: Growth history and sector-dependent impurity incorporation. *Diam. Relat. Mater.* 2004, 13, 1658–1673.
39. Howell, D.; Griffin, W.L.; Piazolo, S.A.; Say, J.M.; Stern, R.A.; Stachel, T.; Nasdala, L.; Rabeau, J.R.; Pearson, N.J.; O'Reilly, S.Y. A spectroscopic and carbon-isotope study of mixed-habit diamonds: Impurity characteristics and growth environment. *Am. Mineral.* 2013, 98, 66–77.
40. Vasilev, E.; Petrovsky, V.; Kozlov, A.; Antonov, A.; Kudriavtsev, A.; Orekhova, K. The story of one diamond: The heterogeneous distribution of the optical centres within a diamond crystal from the Ichetju placer, northern Urals. *Miner Mag.* 2019, 4, 515–522.
41. Zedgenizov, D.A.; Kalinin, A.A.; Kalinina, V.V.; Palyanov, Y.N.; Shatsky, V.S. Nitrogen and hydrogen aggregation in natural octahedral and cuboid diamonds. *Geochem. J.* 2017, 51, 181–192.

Retrieved from <https://encyclopedia.pub/entry/history/show/44106>